Available online at www.sciencedirect.com
ScienceDirect
Comput. Methods Appl. Mech. Engrg. 293 (2015) 170–190
Computer methods in applied mechanics and engineering
www.elsevier.com/locate/cma

An immersed discontinuous finite element method for Stokes interface problems

Slimane Adjerid*, Nabil Chaabane, Tao Lin

Department of Mathematics, Virginia Tech, Blacksburg, VA 24061, USA

Received 14 January 2015; received in revised form 19 April 2015; accepted 22 April 2015
Available online 7 May 2015

Abstract

We present a discontinuous immersed finite element (IFE) method for Stokes interface problems on Cartesian meshes that do not require the mesh to be aligned with the interface. As such, the method allows unfitted meshes with elements cut by the interface and thus, may contain more than one fluid. On these unfitted meshes we construct an immersed Q_1/Q_0 finite element space according to the location of the interface and pertinent interface jump conditions. The proposed Q_1/Q_0 IFE shape functions have several desirable features such as the unisolvence and the partition of unity. We present several numerical examples to demonstrate that the proposed IFE spaces maintain the optimal approximation capability with respect to the polynomials used. We also show that related discontinuous IFE solutions of Stokes interface problems maintain the optimal convergence rates in both L^2 and broken H^1 norms.

Keywords: Immersed finite elements; Discontinuous Galerkin method; Interface problem; Stokes problem

1. Introduction

Physical phenomena in a domain consisting of multiple materials or fluids with an interface are often modeled by differential equations with discontinuous coefficients which are often called interface problems. Solutions to interface problems are often required to satisfy jump conditions across the material interfaces in addition to the pertinent differential equations and the related boundary conditions. Conventional finite element methods with body-fitted meshes can be used to solve interface problems with standard problem-independent finite element shape functions. In general, optimal convergence rates for conventional finite element solutions are attained for fitted meshes where every element essentially contains one material [1–3]. However, This restriction leads to drawbacks such as

1. Excessive remeshing for problems with moving interfaces. The same difficulty occurs for problems with random interfaces where many interface problems of the same type need to be solved with different interfaces corresponding to different values of the parameters in order to estimate quantities of interest such as the expected solution.

* Corresponding author. Tel.: +1 540 231 5945; fax: +1 540 231 5960.
E-mail address: adjerids@math.vt.edu (S. Adjerid).

http://dx.doi.org/10.1016/j.cma.2015.04.006
0045-7825/

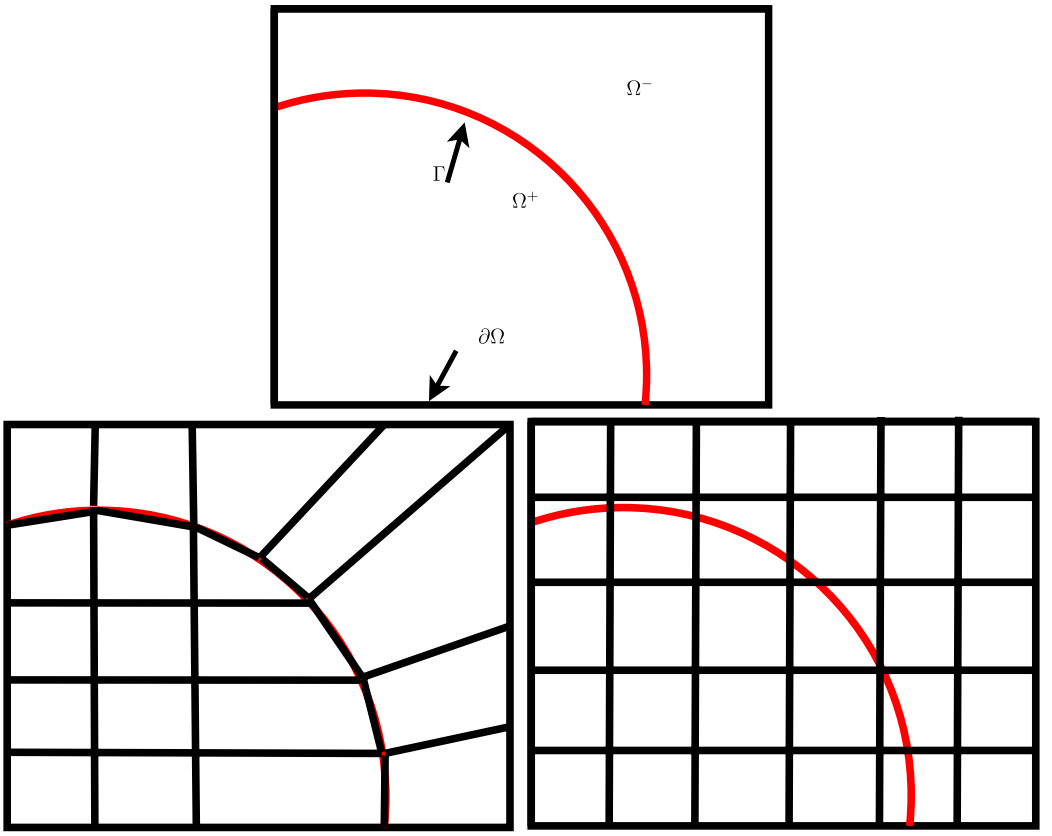

Fig. 1. A rectangular domain Ω cut by an interface Γ (top), a body-fitted mesh according to the interface (bottom left), an interface independent Cartesian mesh (bottom right).

2. Excessive mesh refinement to resolve small structures in the domain such as thin layers.
3. Prohibition of the use of uniform meshes to solve problems with nontrivial interfaces.

In this manuscript we consider the Stokes problem that consists of finding $\mathbf{u}$ and p such that

$$-\nabla \cdot S(\mathbf{u}, p) = \mathbf{f}, \quad \text{in } \Omega \setminus \Gamma, \tag{1.1a}$$

$$\nabla \cdot \mathbf{u} = 0, \quad \text{in } \Omega \setminus \Gamma, \tag{1.1b}$$

$$\mathbf{u} = \mathbf{g}, \quad \text{on } \partial\Omega, \tag{1.1c}$$

where the stress tensor $S_{ij}(\mathbf{u}, p)$ [4] in terms of the velocity $\mathbf{u} = (u_1, u_2)^t$ and pressure p is given by

$$S_{ij}(\mathbf{u}, p) = \nu \boldsymbol{\epsilon}(\mathbf{u})_{ij} - p\delta_{ij}, \quad i, j = 1, 2 \quad \text{with } \boldsymbol{\epsilon}(\mathbf{u})_{ij} = \frac{\partial u_i}{\partial x_j} + \frac{\partial u_j}{\partial x_i}, \tag{1.1d}$$

where δ_{ij} is the Kronecker symbol.

Here, without loss of generality, we assume that the domain Ω is bounded in $\mathbb{R}^2$ with boundary $\partial\Omega$ and it is occupied by two fluids with different viscosities $\nu^{\pm}$. Furthermore, we assume that the domain is separated by an interface Γ into two sub-domains Ω^+ and Ω^- such that each sub-domain contains one fluid as illustrated in Fig. 1. Also, we assume the viscosity ν to be piecewise constant

$$\nu = \begin{cases} \nu^- & \text{in } \Omega^-, \\ \nu^+ & \text{in } \Omega^+, \end{cases} \tag{1.1e}$$

where $\nu^+, \nu^- > 0$.

The physical jump conditions across the interface Γ are

$$[S(\mathbf{u}, p)\mathbf{n}]|_{\Gamma} = \boldsymbol{\sigma}, \tag{1.1f}$$

$$[\mathbf{u}]\,|_{\Gamma} = 0, \tag{1.1g}$$

where $\mathbf{n}$ is the unit normal vector to the interface Γ, $\boldsymbol{\sigma} = [\sigma_1, \sigma_2]^t$ is the surface force and $[\mathbf{v}]_{\Gamma} = \mathbf{v}^+|_{\Gamma} - \mathbf{v}^-|_{\Gamma}$, for a piecewise function $\mathbf{v}$ such that $\mathbf{v}|_{\Omega^{\pm}} = \mathbf{v}^{\pm}$.

The Stokes interface problem described by (1.1) with discontinuous solutions has been a focus of many research articles. Brackbill et al. [5] removed the discontinuity by smoothing out the interface leading to a method that requires finer meshes near interfaces due to its reduced accuracy near the interface. In order to avoid this difficulty, Buscaglia et al. [6] designed a finite element basis for the pressure that models jumps of the normal component of the surface force assuming the tangential component of the surface force to be continuous. They showed through numerical examples that the interpolation error in the pressure is $O(h^{3/2})$ accurate with first-degree polynomials for the pressure. Reusken [7] developed a modified XFEM space by deleting finite element basis functions having small support which improves the conditioning of the resulting system. Reusken proved that the modified XFEM space is as accurate as the standard XFEM space but with better stability properties. However, these XFEM spaces have to be carefully constructed to preserve accuracy. Belytschko and Fries [8] proposed a generalized/extended finite element method that may be applied to problems whose solutions are not smooth. An alternative method was proposed by Becker et al. [9] by considering two discrete solutions one on each of the enlarged sub-domains Ω^+ and Ω^-, then by enforcing the jump conditions weakly using a variant of Nitsche's method. Like the XFEM method, this method may suffer from ill-conditioning depending on the location of the interface. Hansbo et al. [10] were able to circumvent the difficulties faced in the latter method by slightly changing the variational formulation. They proved optimal order of convergence as well as the well-conditioning of the stiffness matrix. The relatively new discontinuous Galerkin method has also been applied to the Stokes interface problem [11] using piecewise polynomials of degree k for velocity and of degree $k-1$ for pressure on body-fitted meshes. They established optimal order of convergence in the L^2 and energy norms, respectively, for pressure and velocity.

Although our focus here is on finite element methods, we would like to note that several immersed finite difference methods have also been developed to solve interface problems and the reader may consult [12–17] and the references therein. For the Stokes problem Li et al. [18] decoupled the velocity and pressure and used an immersed finite difference method to solve for each variable separately.

In this paper, we extend the immersed finite element (IFE) method to the Stokes interface problem. Several immersed finite element methods and spaces have been proposed for solving elliptic problems over the last fifteen years. For a full discussion of existing immersed finite element methods see [19–29] and the references therein. The key idea of the IFE method is to mesh the domain independently of the interface location and allow elements to be intersected by the interface as shown in Fig. 1. The finite element space consists of piecewise polynomial functions which are defined by polynomials on elements that are not cut by the interface and by piecewise polynomial functions satisfying the interface conditions on elements cut by the interface.

The main motivation for the IFE method is to avoid body-fitted meshes which can be cumbersome when the interface geometry is complicated and when dealing with moving interfaces which will require moving meshes. Furthermore, having the possibility to use Cartesian meshes whenever the geometry of the domain allows is also a feature desirable for many applications. However, the standard finite element spaces are no longer capable of capturing the singularities in the solutions; thus, the need for more suitable finite element spaces such as the immersed finite element spaces.

The finite element method proposed in this manuscript has been used to solve Stokes interface problems with moving interfaces [30]. The algorithm consists of creating a coarse background mesh which may be refined, if needed, by subdividing elements cut by the interface. We construct the corresponding IFE space and solve the Stokes interface problem to obtain the velocity and pressure. The velocity is then used to move the interface using an adaptive time integrator. Once the updated location of the interface is determined, the same steps are repeated until, for instance, equilibrium is reached.

The outline of this paper is as follows. We construct the Q_1/Q_0 IFE shape functions and establish their existence and their properties in Section 2. We then present a discontinuous immersed finite element method for solving the Stokes interface problem in Section 3. We perform several computational experiments and present numerical results

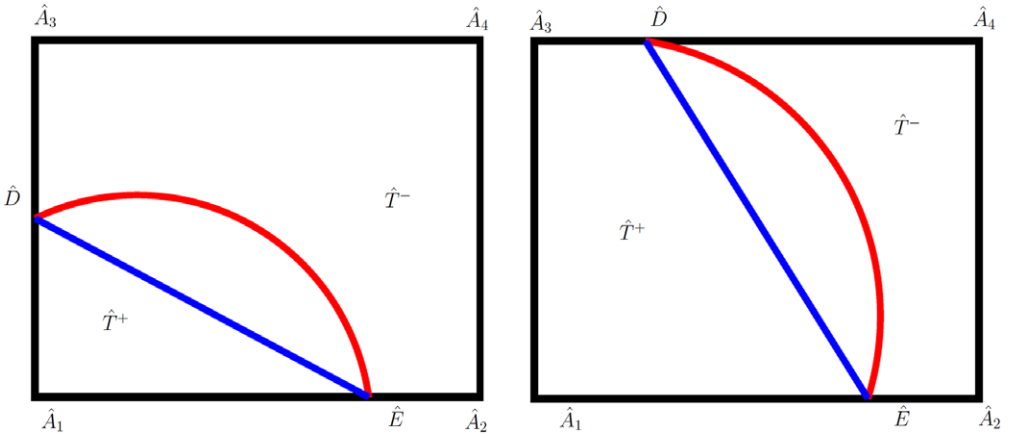

Fig. 2. Reference interface elements of Type I (left) and Type II (right).

in Section 4 to show the approximation properties of the proposed IFE spaces and the convergence properties of our immersed discontinuous finite element method. We conclude with a few remarks in Section 5.

2. IFE spaces for Stokes interface problems

In this section, we develop immersed finite element spaces for Stokes interface problems without surface force and with surface force. Since the velocity $\mathbf{u}$ and the pressure p are not smooth across the interface, the standard finite element functions cannot capture solution singularities on interface elements in non-fitted meshes. First, we design an immersed finite element space for the velocity and pressure by extending the Q_1/Q_0 space on non-interface elements to interface elements. The proposed Q_1/Q_0 IFE space uses piecewise bilinear polynomial approximations for the velocity and piecewise constant approximations for the pressure. Next we discuss how to construct the IFE shape functions on interface elements.

2.1. Q_1/Q_0 IFE shape functions without surface force

Let $\mathcal{T}_h$ be an arbitrary uniform rectangular partition of the domain Ω. Elements of the mesh $\mathcal{T}_h$ that are cut by the interface are called interface elements; otherwise, they are called non-interface elements. Let $\mathcal{T}_h^i$, $\mathcal{T}_h^n$, respectively, denote the set of all interface elements and non-interface elements with $\mathcal{T}_h^n = \mathcal{T}_h \setminus \mathcal{T}_h^i$. We assume that the interface intersects at most two edges of any given element and we consider an element to be a non-interface element when the interface intersects an edge at either one vertex, two adjacent vertices or this whole edge lies on the interface.

Topologically, there are two types of interface elements. The Type I interface elements are those with two adjacent edges cut by the interface and Type II interface elements are with two opposite edges cut by the interface, see the illustrations in Fig. 2. Specifically, let us consider a typical interface rectangular element $T = \square A_1A_2A_3A_4 \in \mathcal{T}_h^i$ with vertices $A_i = (x_i, y_i)^t$, $i = 1, 2, 3, 4$ such that the interface Γ intersects two edges at $D = (x_D, y_D)^t$ and $E = (x_E, y_E)^t$ referred to as interface points. We then approximate the interface $\widetilde{DE} = \Gamma \cap T$ by the line segment $\overline{DE}$ which separates T into two polygonal sub-elements T^+ and T^- such that T^+ contains vertices of T that are in Ω^+. Our plan is to develop IFE functions on T in forms of piecewise bilinear or piecewise constant polynomials defined according to these two sub-elements for approximating the velocity and pressure, respectively, in Stokes interface problems. Note that the approximation capability of bilinear or constant polynomials is capped by $O(h^2)$. Hence, using the linear segment $\overline{DE}$ to approximate $\widetilde{DE} = \Gamma \cap T$ is natural because of its $O(h^2)$ accuracy provided that $\widetilde{DE} = \Gamma \cap T$ is smooth enough. Also, we note that partitioning an interface element T according to the line segment $\overline{DE}$ instead of the original interface curve $\widetilde{DE} = \Gamma \cap T$ has been used in developing IFE functions based on piecewise linear or bilinear polynomials for other types of interface problems [24,27,31].

As usual, the construction and analysis of the finite element shape functions are performed on the reference element $\hat{T} = \square\hat{A}_1\hat{A}_2\hat{A}_3\hat{A}_4$ with vertices $\hat{A}_1 = (0, 0)^t$, $\hat{A}_2 = (1, 0)^t$, $\hat{A}_3 = (0, 1)^t$, $\hat{A}_4 = (1, 1)^t$. Let $X = (x, y)^t$ and

$\hat{X} = (\hat{x}, \hat{y})^t$ and let

$$\hat{X} = F(X) = MX + B, \tag{2.1}$$

be the standard affine mapping from an arbitrary element T to the reference element $\hat{T}$ such that $\hat{A}_i = F(A_i),\ i = 1, 2, 3, 4$. We further note that each interface element T of Type I (Type II) is mapped into a reference element of Type I (Type II) shown in Fig. 2 where $\hat{E} = F(E)$ and $\hat{D} = F(D)$ and $\overline{\hat{D}\hat{E}} = F(\overline{DE})$. The interface points $\hat{E}$ and $\hat{D}$ can be written as

$$\hat{D} = \begin{pmatrix} 0 \\ \hat{d} \end{pmatrix}, \qquad \hat{E} = \begin{pmatrix} \hat{e} \\ 0 \end{pmatrix}, \tag{2.2}$$

for an element of Type I and

$$\hat{D} = \begin{pmatrix} \hat{d} \\ 1 \end{pmatrix}, \qquad \hat{E} = \begin{pmatrix} \hat{e} \\ 0 \end{pmatrix}, \tag{2.3}$$

for an element of Type II, where $0 < \hat{d}, \hat{e} \leq 1$ as shown in Fig. 2.

In this manuscript we are interested in piecewise bilinear (velocity) and constant (pressure) finite elements. Thus, a piecewise linear approximation of the domain boundary may also be used which means that an affine mapping is used for all elements. However, for higher order approximations boundary elements with curved edges and non affine mappings must be used.

Now we are ready to describe our procedure for constructing the IFE shape functions on the reference element. As usual again, a function $\hat{f}(\hat{x}, \hat{y})$ defined for $(\hat{x}, \hat{y}) \in \hat{T}$ leads to a function $f(x, y) = \hat{f}(F(x, y))$ for $(x, y) \in T$ by the affine mapping between the reference element $\hat{T}$ and element T. We first note that the velocity $\mathbf{u}$ and the pressure p are coupled through the jump condition (1.1f) which requires the design of vector-valued shape functions for both of them. This means we plan to approximate the solution vector $\hat{\mathbf{U}} = [\hat{\mathbf{u}}, \hat{p}]^t$ by an IFE function $\hat{\mathbf{\Phi}}$ which is a piecewise polynomial vector function of the form

$$\hat{\mathbf{\Phi}}(\hat{x}, \hat{y}) = \hat{\mathbf{\Phi}}^s(\hat{x}, \hat{y}) = \begin{pmatrix} \hat{\phi}_1^s(\hat{x}, \hat{y}) \\ \hat{\phi}_2^s(\hat{x}, \hat{y}) \\ \hat{\phi}_3^s(\hat{x}, \hat{y}) \end{pmatrix}, \quad \text{for } (\hat{x}, \hat{y})^t \in T^s,\ s = +, -, \tag{2.4a}$$

where

$$\hat{\phi}_j^s(\hat{x}, \hat{y}) = a_j^s + b_j^s \hat{x} + c_j^s \hat{y} + d_j^s \hat{x}\hat{y}, \quad j = 1, 2,\ s = +, -, \tag{2.4b}$$

$$\hat{\phi}_3^s(\hat{x}, \hat{y}) = a_3^s, \quad s = +, -. \tag{2.4c}$$

Next we let $\hat{\mathbf{\Theta}} = (\hat{\phi}_1, \hat{\phi}_2)^t$ such that $\hat{\mathbf{\Theta}}|_{T^s}(\hat{x}, \hat{y}) = \hat{\mathbf{\Theta}}^s(\hat{x}, \hat{y}) = \begin{pmatrix} \hat{\phi}_1^s(\hat{x}, \hat{y}) \\ \hat{\phi}_2^s(\hat{x}, \hat{y}) \end{pmatrix},\ s = +, -$.

We then discuss the construction of IFE shape functions that will be used to form the local IFE space on the reference element $\hat{T}$. According to (2.4) each IFE function is defined by 18 coefficients $a_j^s, b_j^s, c_j^s, d_j^s,\ j = 1, 2,\ s = +, -$ and $a_3^s,\ s = +, -$. Hence, we can define IFE shape functions $\hat{\mathbf{\Phi}}_i,\ i = 1, 2, \ldots, 9$ whose coefficients are determined by the following 18 conditions:

- the continuity of the velocity component across $\overline{\hat{D}\hat{E}}$ for $\hat{\mathbf{\Theta}}_i = (\hat{\phi}_{1,i}, \hat{\phi}_{2,i})^t$

$$\hat{\mathbf{\Theta}}_i^-(\hat{E}) = \hat{\mathbf{\Theta}}_i^+(\hat{E}), \qquad \hat{\mathbf{\Theta}}_i^-(\hat{D}) = \hat{\mathbf{\Theta}}_i^+(\hat{D}), \qquad \frac{\partial^2 \hat{\mathbf{\Theta}}_i^-}{\partial \hat{x} \partial \hat{y}} = \frac{\partial^2 \hat{\mathbf{\Theta}}_i^+}{\partial \hat{x} \partial \hat{y}}, \tag{2.5a}$$

- the weak continuity of the normal stress across $\overline{\hat{D}\hat{E}}$

$$\int_{\overline{\hat{D}\hat{E}}} [S(\hat{\mathbf{\Theta}}_i, \hat{\phi}_{3,i})\mathbf{n}_{\overline{\hat{D}\hat{E}}}] ds = 0, \tag{2.5b}$$

- the continuity of the divergence of the velocity

$$\nabla \cdot \hat{\mathbf{\Theta}}_i^+(\hat{D}) = \nabla \cdot \hat{\mathbf{\Theta}}_i^-(\hat{D}), \tag{2.5c}$$

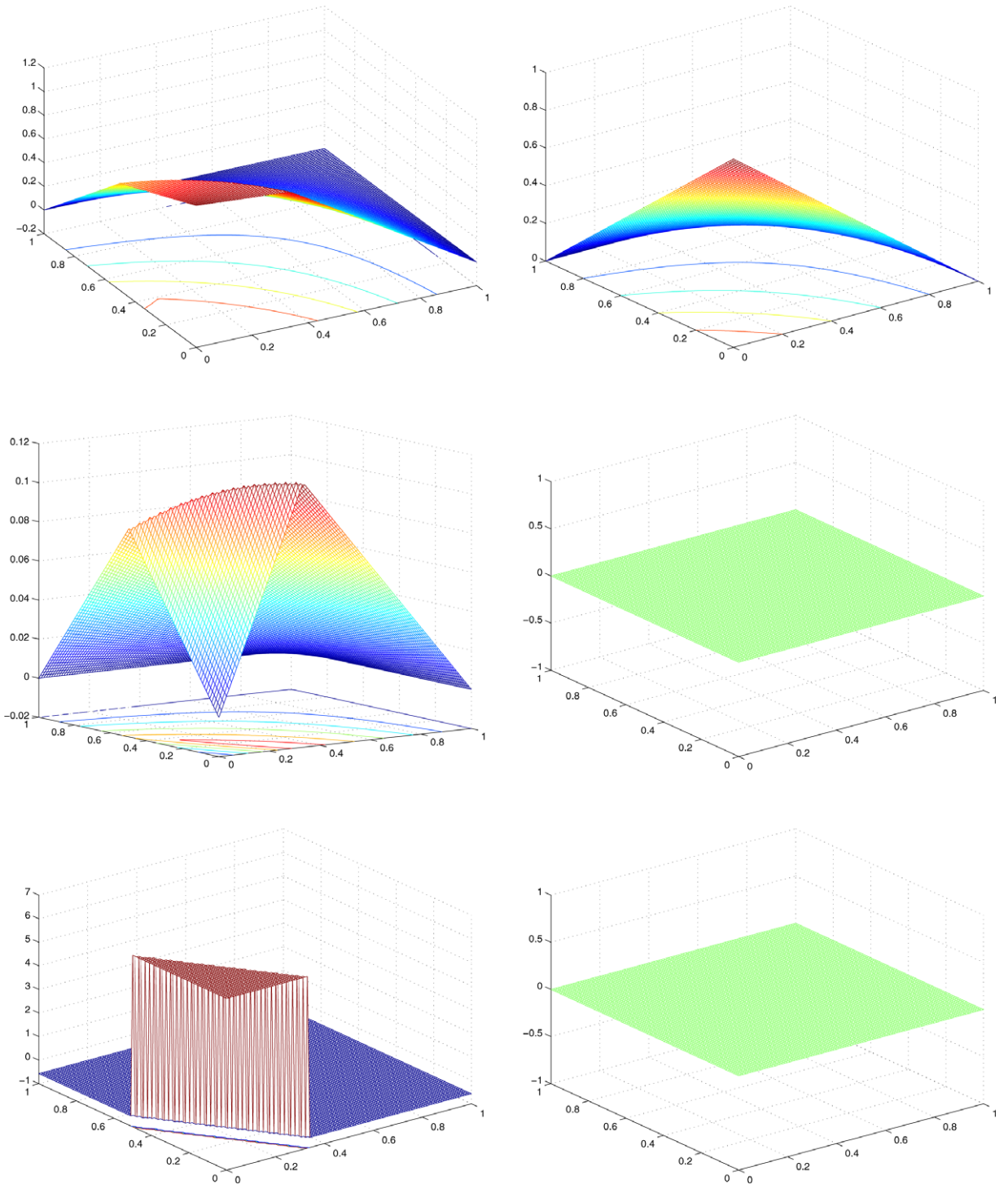

Fig. 3. The (u, v, p) Components of the IFE shape function $\boldsymbol{\Phi}_1$ (left) and standard shape function $\boldsymbol{\Psi}_1$ (right).

- Lagrange and scaling conditions

$$\hat{\phi}_{1,i}(\hat{A}_j) = \delta_{ij}, \qquad \hat{\phi}_{2,i}(\hat{A}_j) = \delta_{i\ j+4}, \quad j = 1, 2, 3, 4, \quad \text{and} \quad \frac{1}{|T|}\int_T \hat{\phi}_{3,i} = \delta_{i9}. \tag{2.5d}$$

Note that the continuity of the second derivatives in (2.5a) is equivalent to $d_1^+ = d_1^-$ and $d_2^+ = d_2^-$ which by using $d_1^+ = d_1^- = d_1$ and $d_2^+ = d_2^- = d_2$ in (2.4a)–(2.4b) reduces the number of unknown coefficients to 16.

Conditions (2.5a)–(2.5d) lead to a linear system $\mathbf{Mc} = \mathbf{b}$ for the coefficient vector $\mathbf{c} = (a_1^+, b_1^+, c_1^+, d_1, a_1^-, b_1^-, c_1^-, a_2^+, b_2^+, c_2^+, d_2, a_2^-, b_2^-, c_2^-, a_3^-, a_3^+)^t$. The matrix $\mathbf{M}$ for Type I element is

$$\begin{pmatrix}
1 & \hat{e} & 0 & 0 & -1 & -\hat{e} & 0 & 0 & 0 & 0 & 0 & 0 & 0 & 0 & 0 & 0 \\
1 & 0 & \hat{d} & 0 & -1 & 0 & -\hat{d} & 0 & 0 & 0 & 0 & 0 & 0 & 0 & 0 & 0 \\
0 & 0 & 0 & 0 & 0 & 0 & 0 & 1 & \hat{e} & 0 & 0 & -1 & -\hat{e} & 0 & 0 & 0 \\
0 & 0 & 0 & 0 & 0 & 0 & 0 & 1 & 0 & d & 0 & -1 & 0 & -\hat{d} & 0 & 0 \\
0 & m_{52} & m_{53} & m_{54} & 0 & m_{56} & \nu^-\hat{e} & 0 & -\nu^+\hat{e} & 0 & m_{511} & 0 & \nu^-\hat{e} & 0 & -\hat{d} & \hat{d} \\
0 & 0 & m_{63} & m_{64} & 0 & 0 & \nu^-\hat{d} & 0 & -\nu^+\hat{d} & m_{610} & m_{611} & 0 & \nu^-\hat{d} & m_{614} & -\hat{e} & \hat{e} \\
0 & 0 & 0 & 0 & 1 & 0 & 0 & 0 & 0 & 0 & 0 & 0 & 0 & 0 & 0 & 0 \\
1 & 1 & 0 & 0 & 0 & 0 & 0 & 0 & 0 & 0 & 0 & 0 & 0 & 0 & 0 & 0 \\
1 & 0 & 1 & 0 & 0 & 0 & 0 & 0 & 0 & 0 & 0 & 0 & 0 & 0 & 0 & 0 \\
1 & 1 & 1 & 1 & 0 & 0 & 0 & 0 & 0 & 0 & 0 & 0 & 0 & 0 & 0 & 0 \\
0 & 0 & 0 & 0 & 0 & 0 & 0 & 0 & 0 & 0 & 0 & 1 & 0 & 0 & 0 & 0 \\
0 & 0 & 0 & 0 & 0 & 0 & 0 & 1 & 1 & 0 & 0 & 0 & 0 & 0 & 0 & 0 \\
0 & 0 & 0 & 0 & 0 & 0 & 0 & 1 & 0 & 1 & 0 & 0 & 0 & 0 & 0 & 0 \\
0 & 0 & 0 & 0 & 0 & 0 & 0 & 1 & 1 & 1 & 1 & 0 & 0 & 0 & 0 & 0 \\
0 & 0 & 0 & 0 & 0 & 0 & 0 & 0 & 0 & 0 & 0 & 0 & 0 & 0 & m_{1515} & m_{1516} \\
0 & -1 & 0 & 0 & 0 & 1 & 0 & 0 & 0 & -1 & 0 & 0 & 0 & 1 & 0 & 0
\end{pmatrix}, \quad (2.6)$$

where

$$m_{52} = -2\nu^+\hat{d}, \qquad m_{53} = -\nu^+\hat{e}, \qquad m_{54} = \frac{1}{2}(\nu^- - \nu^+)\left(\hat{e}^2 + 2\hat{d}^2\right), \qquad m_{56} = 2\nu^-\hat{d},$$

$$m_{511} = \frac{1}{2}(\nu^- - \nu^+)\hat{e}\hat{d},$$

$$m_{63} = -\nu^+\hat{d}, \qquad m_{64} = \frac{1}{2}(\nu^- - \nu^+)\hat{e}\hat{d}, \qquad m_{610} = -2\nu^+\hat{e},$$

$$m_{611} = \frac{1}{2}(\nu^- - \nu^+)\left(2\hat{e}^2 + \hat{d}^2\right), \qquad m_{614} = 2\nu^-\hat{e},$$

$$m_{1515} = \frac{1}{2}\hat{e}\hat{d}, \qquad m_{1516} = 1 - \frac{1}{2}\hat{e}\hat{d}.$$

For an element of Type II the matrix $\mathbf{M}$ is

$$\begin{pmatrix}
1 & \hat{e} & 0 & 0 & -1 & -\hat{e} & 0 & 0 & 0 & 0 & 0 & 0 & 0 & 0 & 0 & 0 \\
1 & d & 1 & 0 & -1 & -\hat{d} & -1 & 0 & 0 & 0 & 0 & 0 & 0 & 0 & 0 & 0 \\
0 & 0 & 0 & 0 & 0 & 0 & 0 & 1 & \hat{e} & 0 & 0 & -1 & -\hat{e} & 0 & 0 & 0 \\
0 & 0 & 0 & 0 & 0 & 0 & 0 & 1 & \hat{d} & 1 & 0 & -1 & -\hat{d} & -1 & 0 & 0 \\
0 & -2\nu^+ & m_{53} & m_{54} & 0 & 2\nu^- & m_{57} & 0 & m_{59} & 0 & m_{510} & 0 & m_{513} & 0 & -1 & 1 \\
0 & 0 & -\nu^+ & m_{64} & 0 & 0 & \nu^- & 0 & -\nu^+ & m_{610} & m_{611} & 0 & \nu^- & m_{614} & \hat{d} - \hat{e} & m_{616} \\
0 & 0 & 0 & 0 & 1 & 0 & 0 & 0 & 0 & 0 & 0 & 0 & 0 & 0 & 0 & 0 \\
1 & 1 & 0 & 0 & 0 & 0 & 0 & 0 & 0 & 0 & 0 & 0 & 0 & 0 & 0 & 0 \\
0 & 0 & 0 & 0 & 1 & 0 & 1 & 0 & 0 & 0 & 0 & 0 & 0 & 0 & 0 & 0 \\
1 & 1 & 1 & 1 & 0 & 0 & 0 & 0 & 0 & 0 & 0 & 0 & 0 & 0 & 0 & 0 \\
0 & 0 & 0 & 0 & 0 & 0 & 0 & 0 & 0 & 0 & 0 & 1 & 0 & 0 & 0 & 0 \\
0 & 0 & 0 & 0 & 0 & 0 & 0 & 1 & 1 & 0 & 0 & 0 & 0 & 0 & 0 & 0 \\
0 & 0 & 0 & 0 & 0 & 0 & 0 & 0 & 0 & 0 & 0 & 1 & 0 & 1 & 0 & 0 \\
0 & 0 & 0 & 0 & 0 & 0 & 0 & 1 & 1 & 1 & 1 & 0 & 0 & 0 & 0 & 0 \\
0 & 0 & 0 & 0 & 0 & 0 & 0 & 0 & 0 & 0 & 0 & 0 & 0 & 0 & \frac{\hat{d} + \hat{e}}{2} & m_{1516} \\
0 & -1 & 0 & 0 & 0 & 1 & 0 & 0 & 0 & -1 & 0 & 0 & 0 & 1 & 0 & 0
\end{pmatrix}, \quad (2.7)$$

$$m_{53} = \nu^+(\hat{d} - \hat{e}), \qquad m_{54} = -\frac{1}{2}(\nu^- - \nu^+)\left(-2 + \hat{d}^2 - \hat{e}^2\right), \qquad m_{57} = \nu^-(-\hat{d} + \hat{e}),$$

$$m_{5,9} = \nu^+(\hat{d} - \hat{e}),$$
$$m_{511} = -\frac{1}{2}(\nu^- - \nu^+)(\hat{d} - \hat{e}), \qquad m_{513} = \nu^-(-\hat{d} + \hat{e}),$$
$$m_{64} = \frac{1}{2}(\nu^- - \nu^+)(\hat{d} + \hat{e}), \qquad m_{610} = 2\nu^+(\hat{d} - \hat{e}), \qquad m_{611} = -\frac{1}{2}(\nu^- - \nu^+)\left(-1 + 2\hat{d}^2 - 2\hat{e}^2\right),$$
$$m_{614} = 2\nu^-(-\hat{d} + \hat{e}), \qquad m_{1516} = \frac{1}{2}(2 - \hat{d} - \hat{e}).$$

The right-hand side vector $\mathbf{b}$ is given as

$$\mathbf{b} = (0, 0, 0, 0, 0, 0, \delta_{i1}, \delta_{i2}, \delta_{i3}, \delta_{i4}, \delta_{i5}, \delta_{i6}, \delta_{i7}, \delta_{i8}, \delta_{i9}, 0)^T.$$

Once these IFE shape functions are constructed on the reference element, the standard affine mapping is applied to obtain the corresponding vector IFE shape functions on an interface element T as $\mathbf{\Phi}_i(x, y) = \hat{\mathbf{\Phi}}_i(F(x, y)), \quad i = 1, 2, \ldots, 9$. On every non-interface element T we use the standard finite element shape functions $\mathbf{\Psi}_i$, $i = 1, 2, \ldots, 9$:

$$\mathbf{\Psi}_i = \begin{pmatrix} \psi_i(x, y) \\ 0 \\ 0 \end{pmatrix}, \qquad \mathbf{\Psi}_{i+4} = \begin{pmatrix} 0 \\ \psi_i(x, y) \\ 0 \end{pmatrix}, \qquad \mathbf{\Psi}_9 = \begin{pmatrix} 0 \\ 0 \\ 1 \end{pmatrix}, \quad i = 1, 2, 3, 4,$$

where ψ_i, $i = 1, 2, 3, 4$ are the standard Lagrange bilinear shape functions associated with the vertices of T. Fig. 3 presents illustrations for the shape functions $\mathbf{\Psi}_1$ and $\mathbf{\Phi}_1$. Unlike $\mathbf{\Psi}_1$ used in the standard Q_1/Q_0 finite element space, the components of the IFE shape function $\mathbf{\Phi}_1$ cannot be decoupled, its second and third components are generally not zero.

Then, the shape functions defined above are used to construct the global IFE space on Ω for the Stokes interface problem as follows:

$$S_h(\Omega) = \{\mathbf{U}_h \mid \mathbf{U}_h|_T \in X_h(T)\}, \tag{2.8}$$

where

$$X_h(T) = \begin{cases} \text{span}\{\mathbf{\Phi}_i(x, y), i = 1, 2, \ldots, 9\}, & \text{if } T \in \mathcal{T}_h^i, \\ \text{span}\{\mathbf{\Psi}_i(x, y), i = 1, 2, \ldots, 9\}, & \text{if } T \in \mathcal{T}_h^n. \end{cases}$$

2.2. Q_1/Q_0 particular IFE functions with surface force

In the case where the jump condition (1.1f) is such that $\boldsymbol{\sigma} \neq 0$, we follow [32] to treat the nonhomogeneous term. First, we construct a set of particular IFE functions that can capture the nonhomogeneous term modeling surface force. These particular functions are solely used to construct the IFE solution and will not be included in the test space and; hence, they will not increase the size of the discrete IFE problem.

On each interface element T, the particular IFE functions are defined as

$$\Upsilon_j = \begin{pmatrix} \Lambda_j \\ \psi_j \end{pmatrix}, \quad j = 1, 2,$$

whose velocity component is

$$\Lambda_j(x, y) = \begin{cases} \Lambda_j^+(x, y) & \text{on } T^+ \\ \Lambda_j^-(x, y) & \text{on } T^- \end{cases} \tag{2.9}$$

with

$$\Lambda_j^s(x, y) = \begin{pmatrix} \Lambda_{1,j}^s(x, y) \\ \Lambda_{2,j}^s(x, y) \end{pmatrix}, \quad \text{on } T^s, \ s = +, -, \tag{2.10}$$

and the pressure component is a piecewise constant function such that

$$\psi_j = \begin{cases} \psi_j^+(x,y), & \text{on } T^+, \\ \psi_j^-(x,y), & \text{on } T^-, \end{cases} \quad \psi_j^s(x,y) = c^s,\ s = +,-.$$

We then define the velocity component in particular IFE functions to be piecewise polynomials

$$\Lambda_{i,j}^s(x,y) = a_{i,j}^s + b_{i,j}^s x + c_{i,j}^s y + d_{i,j}^s xy, \quad j = 1,2,\ i = 1,2,\ s = +,-. \tag{2.11}$$

We further require that the particular IFE functions satisfy the following constraints

$$\Lambda_j(A_i) = 0, \quad i = 1,2,3,4, \tag{2.12}$$

$$\Lambda_j^-(E) = \Lambda_j^+(E), \qquad \Lambda_j^-(D) = \Lambda_j^+(D), \qquad \frac{\partial^2 \Lambda_j^-}{\partial x \partial y} = \frac{\partial^2 \Lambda_j^+}{\partial x \partial y}, \tag{2.13}$$

$$\int_{\overline{DE}} [S(\Lambda_j, \psi_j)\mathbf{n}_{\overline{DE}}] ds = \mathbf{e}_j, \quad \mathbf{e}_j \text{ is the canonical vector in } \mathbb{R}^2, \tag{2.14}$$

$$\frac{1}{|T|}\int_T \psi_j dX = 0, \qquad \nabla \cdot \Lambda_j^+(D) = \nabla \cdot \Lambda_j^-(D), \quad j = 1,2. \tag{2.15}$$

Note that these conditions lead to linear systems for determining the parameters of the particular IFE functions and the matrices of these linear systems are given by (2.6) and (2.7), respectively, for Type I and Type II interface elements. The right-hand side is given as

$$\mathbf{b} = (0,0,0,0,\delta_{i1},\delta_{i2},0,0,0,0,0,0,0,0,0,0)^T.$$

For the Stokes interface problem with a nonzero interface surface force $\boldsymbol{\sigma} \neq 0$, its IFE solution $(\mathbf{u}_h, p_h)$ be in the function set $S_h(\Omega) \oplus \{\mathbf{Q}_h(x,y)\}$ where $S_h(\Omega)$ is the IFE space defined in the previous section and the vector function $\mathbf{Q}_h(x,y)$ is such that

$$\mathbf{Q}_h(x,y) = \begin{cases} \kappa_1 \Upsilon_1(x,y) + \kappa_2 \Upsilon_2(x,y), & \text{on T } \in \mathcal{T}_h^i \\ 0 & \text{elsewhere,} \end{cases} \tag{2.16}$$

where $\kappa_j = \int_{\overline{DE}} \boldsymbol{\sigma}_{h,j} dX$ and $\boldsymbol{\sigma}_h$ is the linear interpolation of $\boldsymbol{\sigma}$ defined by $\boldsymbol{\sigma}_h(E) = \boldsymbol{\sigma}(E)$ and $\boldsymbol{\sigma}_h(D) = \boldsymbol{\sigma}(D)$. Hence, the IFE solution on an interface element will take the form

$$\begin{pmatrix} \mathbf{u}_h \\ p_h \end{pmatrix} = \sum_{i=1}^{9} c_i \boldsymbol{\Phi}_i + \kappa_1 \Upsilon_1 + \kappa_2 \Upsilon_2. \tag{2.17}$$

2.3. Basic properties of the bilinear IFE space

In this section, we investigate basic properties of the IFE shape functions for the Stokes interface problem. We start by stating a result on the existence and uniqueness of IFE shape functions for an arbitrary configuration of ν^-, ν^+ and interface location.

Proposition 2.1. *On every interface element T, there exists a unique set of linearly independent IFE shape functions $\{\boldsymbol{\Phi}_i,\ i = 1,2,\ldots,9\}$ as defined in the previous section.*

Proof. The uniqueness and existence of IFE shape functions are directly guaranteed by the invertibility of the matrices (2.6) and (2.7).

For interface elements of Type I, a direct computation of the determinant of the matrix (2.6) yields

$$det(M) = -\frac{1}{2}(\hat{e}^2 + \hat{d}^2)(Q_1\nu^- + Q_2\nu^+), \tag{2.18}$$
$$Q_1 = (-2\hat{e}^2(-1+\hat{d}) + \hat{e}^3\hat{d} + 2\hat{d}^2 + \hat{e}(-2+\hat{d})\hat{d}^2),$$

$$Q_2 = -\hat{e}\hat{d}(-2\hat{e} + \hat{e}^2 + (-2 + \hat{d})\hat{d}).$$

Thus it suffices to show that $Q_1 > 0$ and $Q_2 > 0$. Since $0 < \hat{e}, \hat{d} < 1$ and $\hat{e}^2 \leq \hat{e}$

$$Q_1 > -4\hat{e}\hat{d} + 2\hat{e}^2 + 2\hat{d}^2 + \hat{e}^3\hat{d} + \hat{e}\hat{d}^3.$$

Factoring the first three terms of the right-hand side we obtain

$$Q_1 > 2(\hat{e} - \hat{d})^2 + \hat{e}^3\hat{d} + \hat{e}\hat{d}^3 > 0.$$

Similarly one can easily check that $Q_2 > 0$ by writing Q_2 as

$$Q_2 = -\hat{e}\hat{d}(\hat{e}(-2 + \hat{e}) + (-2 + \hat{d})\hat{d})$$

and noting that both $(-2 + \hat{d})\hat{d} < 0$ and $(-2 + \hat{e})\hat{e} < 0$. This leads to $Q_2 > 0$. Hence, $det(M) \neq 0$, for all $\hat{e}, \hat{d} \in (0, 1)$.

For interface elements of Type II, the determinant of the matrix M in (2.7) is such that

$$det(M) = -\frac{1}{2}(1 + \hat{d}^2 - 2\hat{d}\hat{e} + \hat{e}^2)(P_1\nu^- + P_2\nu^+), \tag{2.19}$$

where

$$P_1 = (2 + \hat{d}^3 - \hat{e} - \hat{d}^2\hat{e} + \hat{e}^3 - \hat{d}(1 + \hat{e}^2)),$$
$$P_2 = (-\hat{d}^3 + \hat{e} + 2\hat{e}^2 - \hat{e}^3 + \hat{d}^2(2 + \hat{e}) + \hat{d}(1 - 4\hat{e} + \hat{e}^2)).$$

First, we can write P_1 as

$$P_1 = 2 + \hat{d}^3 + \hat{e}^3 - \hat{e} - \hat{d} - \hat{e}^2\hat{d} - \hat{e}\hat{d}^2,$$

and noting that $-\hat{e}^2\hat{d} > -\hat{e}\hat{d}$ and $-\hat{e}\hat{d}^2 > -\hat{e}\hat{d}$, we obtain

$$P_1 > 2 + \hat{d}^3 + \hat{e}^3 - \hat{e} - \hat{d} - 2\hat{e}\hat{d}.$$

Applying $2\hat{e}\hat{d} < \hat{e}^2 + \hat{d}^2$ we obtain

$$P_1 > 2 + \hat{d}(\hat{d}^2 - \hat{d} - 1) + \hat{e}(\hat{e}^2 - \hat{e} - 1).$$

Since $-1 < x(x^2 - x - 1) < 0$, for $0 < x < 1$ we establish $P_1 > 0$.

Next, we write P_2 as follows:

$$P_2 = -\hat{d}^3 + \hat{e} + 2\hat{e}^2 - \hat{e}^3 + 2\hat{d}^2 + \hat{d}^2\hat{e} + \hat{d} - 4\hat{d}\hat{e} + \hat{d}\hat{e}^2.$$

Note that $\hat{e} > \hat{e}^3$ and $\hat{d} > \hat{d}^3$, thus

$$P_2 > 2\hat{e}^2 + 2\hat{d}^2 + \hat{e}\hat{d}^2 + \hat{d}\hat{e}^2 - 4\hat{d}\hat{e} = 2(\hat{e} - \hat{d})^2 + \hat{e}\hat{d}^2 + \hat{d}\hat{e}^2 > 0.$$

Therefore $det(M) \neq 0, \ \forall \ 0 < \hat{e}, \hat{d} < 1.$ □

In the next proposition we show that the velocity component of an IFE function is continuous on each element.

Proposition 2.2. *The velocity component of an IFE function is continuous on each element.*

Proof. The statement is obviously true on each non-interface element because the standard bilinear shape functions are all continuous. On each interface element, the arguments in Proposition 4.1 of [31] can be applied here to show the continuity of the velocity component of each IFE shape function is continuous and this results in the needed proof. □

The next result is easy to verify.

Proposition 2.3. *The IFE Q_1/Q_0 space $S_h(\Omega)$ over a mesh $\mathcal{T}_h$ of Ω defined above has the same dimension as the standard Q_1/Q_0 finite element space on the same mesh.*

Next we show that the IFE shape functions on each interface element form a partition of unity.

Proposition 2.4. *If* $\boldsymbol{\Phi}_i,\ i = 1, 2, \ldots, 9$ *are the IFE shape functions on an interface element, then*

$$\sum_{i=1}^{4} \boldsymbol{\Phi}_i(x, y) = \begin{pmatrix} 1 \\ 0 \\ 0 \end{pmatrix}, \qquad \sum_{i=4}^{8} \boldsymbol{\Phi}_i(x, y) = \begin{pmatrix} 0 \\ 1 \\ 0 \end{pmatrix}, \tag{2.20}$$

$$\boldsymbol{\Phi}_9(x, y) = \begin{pmatrix} 0 \\ 0 \\ 1 \end{pmatrix}, \quad \forall (x, y)^t \in T. \tag{2.21}$$

Proof. The proof is accomplished by a direct verification. □

The next proposition shows that the proposed Q_1/Q_0 IFE shape functions are consistent with the associated standard finite element shape functions.

Proposition 2.5. *If* $v^+ = v^-$ *on an interface element* T*, then the* Q_1/Q_0 *IFE and standard Lagrange* Q_1/Q_0 *finite element shape functions are the same.*

Proof. Noting that, when $v^+ = v^-$, the jump conditions (2.5a)–(2.5d) are satisfied by both the IFE and the standard Q_1/Q_0 shape functions, by uniqueness, these two types of shape functions are equal. □

3. An immersed discontinuous Galerkin method

There exist several discontinuous Galerkin methods for the Stokes problem, either in the mixed [33,34] or in the primal [35,36,11] formulations. Here we use the primal DG formulation in [37] to construct a discontinuous Galerkin immersed finite element (DGIFE) method for the Stokes interface problem. The proposed method uses the standard Q_1/Q_0 space on non-interface elements while the new IFE Q_1/Q_0 space is used on interface elements. The combination of this choice of finite element functions and the DG formulation is natural because of two main reasons: (i) the DG formulation has the desired stability with the Q_1/Q_0 finite elements [37] and (ii) the DG formulation can handle the discontinuity of the Q_1/Q_0 IFE functions across element edges. Furthermore, the standard mixed finite element formulation with Q_1/Q_0 for the Stokes problem is unstable and we expect it to stay unstable with the IFE Q_1/Q_0. For this reason we did not use the mixed formulation. However, for higher degree finite element spaces such as Q_2/Q_1, we expect to find optimal immersed methods based on the mixed formulation. This will be investigated in the future.

Let us recall that the standard Q_1/Q_0 finite element method for the Stokes problem is obtained by partitioning the domain Ω into a Cartesian mesh $\mathcal{T}_h$ and on every element we use standard Lagrange bilinear shape functions for the velocity and constant function for the pressure. Next, let $\mathcal{E}_h$ denote the set of all edges in $\mathcal{T}_h$ and let $\mathcal{E}_h^i \subset \mathcal{E}_h$ be the set of edges cut by the interface and let

$$\mathcal{H}^m(\Omega) = \{(\mathbf{u}, p) : \mathbf{u} \in C^0(\Omega), [S(\mathbf{u}, p)\mathbf{n}]_\Gamma = \boldsymbol{\sigma},\ \mathbf{u} \in \left(H^m(A)\right)^2 \text{ and } p \in H^1(A),\ \ \forall A \subset \Omega^s, s = +, -\},$$

where H^m is the standard Sobolev space and

$$\mathcal{H}_0^m(\Omega) = \{(\mathbf{u}, p) \in \mathcal{H}^m : \boldsymbol{\sigma}|_\Gamma = 0,\ \mathbf{u}|_{\partial\Omega} = 0\}.$$

In order to construct the weak formulation we assume that $(\mathbf{u}, p) \in \mathcal{H}^2(\Omega)$ is the solution of the Stokes problem (1.1). On an arbitrary edge $e \in \mathcal{E}_h$ shared by two elements T^R and T^L we define the average and jump of a function $\mathbf{u}$ across an edge e as

$$\{\mathbf{u}\}_e = \frac{1}{2}(\mathbf{u}|_{T^R} + \mathbf{u}|_{T^L}),$$
$$[\mathbf{u}]_e = (\mathbf{u}|_{T^R} - \mathbf{u}|_{T^L}).$$

On a boundary edge $e \in \partial\Omega$ we define the average and jump by

$$\{\mathbf{u}\}_e = \mathbf{u}|_e,$$

and

$$[\mathbf{u}]_e = \mathbf{u}|_e.$$

Following the standard procedure, see for instance, [37], we multiply the system (1.1) by $(\mathbf{v}, q) \in \mathcal{H}_0^1(\Omega)$ and integrate over an arbitrary non-interface element $T \in \mathcal{T}_h$ to obtain

$$-\int_T (\nabla \cdot S(\mathbf{u}, p)) \cdot \mathbf{v} dx - \int_T \nabla \cdot \mathbf{u} q dx = \int_T \mathbf{f} \cdot \mathbf{v} dx. \tag{3.1}$$

We apply the divergence theorem to integrate the first term by parts and obtain

$$-\int_{\partial T} (S(\mathbf{u}, p)\mathbf{n}) \cdot \mathbf{v} ds + \int_T S(\mathbf{u}, p) : \nabla \mathbf{v} dx - \int_T \nabla \cdot \mathbf{u} q dx = \int_T \mathbf{f} \cdot \mathbf{v} dx, \tag{3.2}$$

where $A : B = \sum_{i=1}^2 \sum_{j=1}^2 A_{ij} B_{ij}$ and $\mathbf{n}$ is the outward unit vector normal to ∂T.

On an interface element T, we apply the divergence theorem on $T \cap \Omega^+$ and $T \cap \Omega^-$ and take into account that the exact solution satisfies the jump conditions (1.1f) and (1.1g) across the interface to obtain

$$-\int_{\partial T} (S(\mathbf{u}, p)\mathbf{n}) \cdot \mathbf{v} ds + \int_T S(\mathbf{u}, p) : \nabla \mathbf{v} dx - \int_T \nabla \cdot \mathbf{u} q dx = \int_T \mathbf{f} \cdot \mathbf{v} dx + \int_{T \cap \Gamma} \boldsymbol{\sigma} \cdot \mathbf{v} ds. \tag{3.3}$$

Summing over all elements leads to

$$-\sum_{T \in \mathcal{T}_h} \int_{\partial T} (S(\mathbf{u}, p)\mathbf{n}) \cdot \mathbf{v} ds + \int_\Omega S(\mathbf{u}, p) : \nabla \mathbf{v} dx - \int_\Omega \nabla \cdot \mathbf{u} q dx = \int_\Omega \mathbf{f} \cdot \mathbf{v} dx + \int_\Gamma \boldsymbol{\sigma} \cdot \mathbf{v} ds. \tag{3.4}$$

Since $(\mathbf{u}, p) \in \mathcal{H}^2(\Omega)$, we obtain

$$-\sum_{e \in \mathcal{E}_h} \int_e [(S(\mathbf{u}, p)\mathbf{n}) \cdot \mathbf{v}] ds + \int_\Omega S(\mathbf{u}, p) : \nabla \mathbf{v} dx - \int_\Omega \nabla \cdot \mathbf{u} q dx = \int_\Omega \mathbf{f} \cdot \mathbf{v} dx + \int_\Gamma \boldsymbol{\sigma} \cdot \mathbf{v} ds. \tag{3.5}$$

Applying the identity $ab - cd = \frac{1}{2}(a + c)(b - d) + \frac{1}{2}(a - c)(b + d)$ yields

$$\begin{aligned} &-\sum_{e \in \mathcal{E}_h} \int_e ([(S(\mathbf{u}, p)\mathbf{n})] \cdot \{\mathbf{v}\} + \{(S(\mathbf{u}, p)\mathbf{n})\} \cdot [\mathbf{v}]) ds \\ &+ \int_\Omega S(\mathbf{u}, p) : \nabla \mathbf{v} dx - \int_\Omega \nabla \cdot \mathbf{u} q dx = \int_\Omega \mathbf{f} \cdot \mathbf{v} dx + \int_\Gamma \boldsymbol{\sigma} \cdot \mathbf{v} ds. \end{aligned} \tag{3.6}$$

Every interface edge can be expressed as $e = e^+ \cup e^-$, where $e^\pm = e \cap \Omega^\pm$. Hence

$$\int_e [S(\mathbf{u}, p)\mathbf{n}] \cdot \{\mathbf{v}\} ds = \int_{e^+} [S(\mathbf{u}, p)\mathbf{n}] \cdot \{\mathbf{v}\} ds + \int_{e^-} [S(\mathbf{u}, p)\mathbf{n}] \cdot \{\mathbf{v}\} ds.$$

Since $(\mathbf{u}, p) \in \mathcal{H}^2(\Omega)$, we write

$$\int_e [S(\mathbf{u}, p)\mathbf{n}] \cdot \{\mathbf{v}\} ds = 0, \tag{3.7}$$

which also holds for non-interface elements.

Combining (3.6) and (3.7) with $(\mathbf{u}, p) \in \mathcal{H}^2(\Omega)$ and assuming $\mathbf{u}$ continuous lead to the interior penalty weak formulation

$$\begin{aligned} &\int_\Omega S(\mathbf{u}, p) : \nabla \mathbf{v} dx - \int_\Omega \nabla \cdot \mathbf{u} q dx - \sum_{e \in \mathcal{E}_h} \int_e \{(S(\mathbf{u}, p)\mathbf{n})\} \cdot [\mathbf{v}] ds \\ &+ \sum_{e \in \mathcal{E}_h} \frac{\alpha}{h_e} \int_e \nu [\mathbf{u}] \cdot [\mathbf{v}] ds + \gamma \sum_{e \in \mathcal{E}_h} \int_e \{(\nu \boldsymbol{\epsilon}(\mathbf{v})\mathbf{n})\} \cdot [\mathbf{u}] ds + \sum_{e \in \mathcal{E}_h} \int_e \{q\}[\mathbf{u}] \cdot \mathbf{n} ds = \int_\Omega \mathbf{f} \cdot \mathbf{v} dx \end{aligned}$$

$$+\int_{\Gamma}\boldsymbol{\sigma}\cdot\mathbf{v}ds+\gamma\sum_{e\subset\partial\Omega}\int_{e}\{(\nu\boldsymbol{\epsilon}(\mathbf{v})\mathbf{n})\}\cdot[\mathbf{g}]ds+\sum_{e\subset\partial\Omega}\frac{\alpha}{h_e}\int_{e}\nu\{q\}[\mathbf{g}]\cdot\mathbf{n}ds$$

$$+\sum_{e\subset\partial\Omega}\frac{\alpha}{h_e}\int_{e}\nu[\mathbf{g}]\cdot[\mathbf{v}]ds, \tag{3.8}$$

where α is a positive stabilization parameter and $\gamma=1$ for the nonsymmetric weak formulation (NIPG) while $\gamma=-1$ for the symmetric weak formulation (SIPG).

The weak form above leads to the interior penalty formulation for the Stokes problem consisting of finding $(\mathbf{u},p)\in\mathcal{H}^1(\Omega)$ such that

$$\begin{cases}A(\mathbf{u},\mathbf{v})+B(\mathbf{v},p)=L(\mathbf{v})\\ B(\mathbf{u},q)=G(q),\end{cases}\qquad\forall(\mathbf{v},q)\in\mathcal{H}_0^1(\Omega), \tag{3.9a}$$

where

$$A(\mathbf{w},\mathbf{v})=\int_{\Omega}\nu\boldsymbol{\epsilon}(\mathbf{w}):\nabla\mathbf{v}dx-\sum_{e\in\mathcal{E}_h}\int_{e}\nu\{\boldsymbol{\epsilon}(\mathbf{w})\mathbf{n}\}\cdot[\mathbf{v}]ds+\gamma\sum_{e\in\mathcal{E}_h}\int_{e}\{\nu\boldsymbol{\epsilon}(\mathbf{v})\mathbf{n}\}\cdot[\mathbf{w}]+\sum_{e\in\mathcal{E}_h}\frac{\alpha}{h_e}\int_{e}\nu[\mathbf{u}]\cdot[\mathbf{v}]ds, \tag{3.9b}$$

$$B(\mathbf{v},q)=-\int_{\Omega}q\nabla\cdot\mathbf{v}dx+\sum_{e\in\mathcal{E}_h}\int_{e}\{q\}[\mathbf{v}]\cdot\mathbf{n}ds. \tag{3.9c}$$

$$L(\mathbf{v})=\int_{\Omega}\mathbf{f}\cdot\mathbf{v}dx+\int_{\Gamma}\boldsymbol{\sigma}\cdot\mathbf{v}ds+\gamma\sum_{e\subset\partial\Omega}\int_{e}\{(\nu\boldsymbol{\epsilon}(\mathbf{v})\mathbf{n})\}\cdot[\mathbf{g}]ds+\sum_{e\subset\partial\Omega}\frac{\alpha}{h_e}\int_{e}\nu[\mathbf{g}]\cdot[\mathbf{v}]ds, \tag{3.9d}$$

$$G(q)=\sum_{e\subset\partial\Omega}\int_{e}\{q\}[\mathbf{g}]\cdot\mathbf{n}ds. \tag{3.9e}$$

Let $V_j,\ j=1,2,\ldots,N_b$, denote the mesh vertices on the boundary $\partial\Omega$ and define the IFE set

$$S_{h,E}(\Omega)=\{(\mathbf{u}_h,p_h)\in S_h(\Omega)\oplus\{\mathbf{Q}_h(x,y)\}:\ \mathbf{u}_h(V_j)=\mathbf{g}(V_j),\ j=1,2,\ldots,N_b\}, \tag{3.10}$$

and the space

$$S_{h,0}(\Omega)=\{(\mathbf{v}_h,q_h)\in S_h(\Omega):\ \mathbf{v}_h(V_j)=0,\ j=1,2,\ldots,N_b\}. \tag{3.11}$$

Then, the DGIFE method consists of finding $(\mathbf{u}_h,p_h)\in S_{h,E}(\Omega)$ such that

$$\begin{cases}A(\mathbf{u}_h,\mathbf{v}_h)+B(\mathbf{v}_h,p_h)=L_h(\mathbf{v}_h)\\ B(\mathbf{u}_h,q_h)=G(q_h),\end{cases}\qquad\forall(\mathbf{v}_h,q_h)\in S_{h,0}(\Omega) \tag{3.12a}$$

where

$$L_h(\mathbf{v}_h)=\int_{\Omega}\mathbf{f}\cdot\mathbf{v}_hdx+\sum_{T\in\mathcal{T}_h^i}\int_{\overline{DE}}\boldsymbol{\sigma}_h\cdot\mathbf{v}_hds+\gamma\sum_{e\subset\partial\Omega}\int_{e}\{(\nu\boldsymbol{\epsilon}(\mathbf{v}_h)\mathbf{n})\}\cdot[\mathbf{g}]ds$$

$$+\sum_{e\subset\partial\Omega}\frac{\alpha}{h_e}\int_{e}\nu[\mathbf{g}]\cdot[\mathbf{v}_h]ds. \tag{3.12b}$$

The last term in (3.12b) is nonzero if, at least, one boundary edge is an interface edge.

4. Computational examples

Here we investigate the approximation properties of the IFE spaces and the convergence properties of the proposed immersed discontinuous Galerkin method for the Stokes problem.

L^2 and H^1 errors on non-interface elements are computed using standard Gauss quadratures. However, extra care is needed near the interface where we assume that every interface element Δ is split by the true interface as

$\Delta = \Delta^+ \cup \Delta^-$. We further assume that the piecewise linear approximate interface split the domain Ω into Ω_h^+ and Ω_h^- and $\Delta = \Delta_h^+ \cup \Delta_h^-$. Here we recall the notation $\Delta^\pm = \Delta \cap \Omega^\pm$ and $\Delta_h^\pm = \Delta \cap \Omega_h^\pm$. For, instance, the true L^2 error of the pressure on such interface element Δ is computed as

$$\|p - p_h\|_{0,\Delta}^2 = \|p^+ - p_h^+\|_{0,\Delta^+\cap\Delta_h^+}^2 + \|p^- - p_h^-\|_{0,\Delta^-\cap\Delta_h^-}^2 + \|p^+ - p_h^-\|_{0,\Delta^+\cap\Delta_h^-}^2 + \|p^- - p_h^+\|_{0,\Delta^-\cap\Delta_h^+}^2.$$

The subregions $\Delta^+ \cap \Delta_h^+$ and $\Delta^- \cap \Delta_h^-$ may be split into triangles with at most one curved side for which suitable quadratures exist. The subregions $\Delta^+ \cap \Delta_h^-$ and $\Delta^- \cap \Delta_h^+$ are bounded by the true interface and its linear approximation. Elementary numerical quadrature methods on such regions can be found in elementary numerical analysis books such as [38].

Since we do not have a convergence theory for the proposed IFE sets and methods, we have carried out extensive numerical experiments to study the effects of using piecewise linear approximations of both the interface and the surface force $\boldsymbol{\sigma}$ and a group of typical examples are presented here. First, we study the interpolation properties of the piecewise polynomial IFE functions by considering three functions. In Example 4.1 we use a function admitting a singularity across a linear interface with $\boldsymbol{\sigma} = \mathbf{0}$. In Example 4.2 we consider a function which is singular across a circular interface with $\boldsymbol{\sigma} = \mathbf{0}$ and finally in Example 4.3 we investigate the approximation capability of our IFE sets using a function which is singular across a circular interface with surface force $\boldsymbol{\sigma} \neq \mathbf{0}$. Furthermore, we study the performance of our IFE sets by applying NIPG and SIPG to three Stokes problems with a linear and a circular interfaces and no surface force. We conclude our experiment by solving the Stokes problem with a circular interface and a nonzero surface force.

4.1. Approximation properties of bilinear IFE functions

First, we investigate the approximation capabilities of our Q_1/Q_0 IFE functions by computing interpolation errors and their convergence rates under mesh refinement.

Here we consider $\mathcal{T}_h$ a Cartesian mesh of the domain Ω and, since we are interested in solving Stokes interface problems, we only test the approximation capabilities of our IFE functions in the set

$$\mathcal{S}(\Omega) = \{(\mathbf{u}, p) \mid [\mathbf{u}]_\Gamma = 0, [S(\mathbf{u}, p)\mathbf{n}]|_\Gamma = \boldsymbol{\sigma}\}.$$

The piecewise polynomial interpolant $\mathbf{I}_h(\mathbf{u}, p) \in S_h(\Omega)$ of a vector function $(\mathbf{u}, p) \in \mathcal{S}(\Omega)$ on an element $T = \square A_1A_2A_3A_4$ is defined by

$$\mathbf{I}_h(\mathbf{u}, p)|_T = \begin{cases} \sum_{i=1}^{4} u_1(A_i)\boldsymbol{\Phi}_i + \sum_{i=5}^{8} u_2(A_{i-4})\boldsymbol{\Phi}_i + p_T\boldsymbol{\Phi}_9 + \sum_{j=1}^{2} \kappa_j \boldsymbol{\Upsilon}_j, & \text{if } T \in \mathcal{T}_h^i, \\ \sum_{i=1}^{4} u_1(A_i)\boldsymbol{\Psi}_i + \sum_{i=5}^{8} u_2(A_{i-4})\boldsymbol{\Psi}_i + p_T\boldsymbol{\Psi}_9, & \text{if } T \in \mathcal{T}_h^n, \end{cases} \tag{4.1}$$

where $p_T = \int_T p dX$, and $\boldsymbol{\Phi}_i$, $\boldsymbol{\Psi}_i$ and $\boldsymbol{\Upsilon}_j$, respectively, are the Q_1/Q_0 IFE shape functions, standard shape functions and particular IFE functions associated with element T. Since the IFE shape functions are coupled, the ith component $\mathbf{I}_h(\mathbf{u}, p)$ denoted by $(\mathbf{I}_h(\mathbf{u}, p))_i$ is such that $(\mathbf{I}_h(\mathbf{u}, p))_1 \approx u_1$, $(\mathbf{I}_h(\mathbf{u}, p))_2 \approx u_2$ and $(\mathbf{I}_h(\mathbf{u}, p))_3 \approx p$ with errors $\epsilon(u_i) = u_i - (\mathbf{I}_h(\mathbf{u}, p))_i$, for $i = 1, 2$ and $\epsilon(p) = p - (\mathbf{I}_h(\mathbf{u}, p))_3$.

Example 4.1. We consider the domain $\Omega = [-1, 1]^2$ cut by the linear interface $y = -x - \sqrt{0.3}$ which splits Ω into $\Omega^+ = \{(x, y)^t : y + x + \sqrt{0.3} > 0\}$ and $\Omega^- = \{(x, y)^t : y + x + \sqrt{0.3} < 0\}$. We select the following function $(\mathbf{u}, p) \in \mathcal{S}(\Omega)$ given by

$$\mathbf{u} = \begin{cases} u_1 = \begin{cases} x^2 + y + y^2, & \text{if } (x, y) \in T^+, \\ \dfrac{-\nu^+(0.3 - x^2 + 2\sqrt{0.3}y + y^2) + \nu^-(0.3 + y + 2\sqrt{0.3}y + 2y^2)}{\nu^-}, & \text{if } (x, y) \in T^-, \end{cases} \\ u_2 = \begin{cases} \dfrac{-2x(x + \nu^- y)}{\nu^-}, & \text{if } (x, y) \in T^+, \\ \dfrac{2x(-x + \nu^-(\sqrt{0.3} + x) - \nu^+(\sqrt{0.3} + x + y))}{\nu^-}, & \text{if } (x, y) \in T^-, \end{cases} \end{cases} \tag{4.2a}$$

Table 1
L^2 interpolation errors for Example 4.1.

N	$\|\epsilon(u_1)\|_{0,\Omega}$	Order	$\|\epsilon(u_2)\|_{0,\Omega}$	Order	$\|\epsilon(p)\|_{0,\Omega}$	Order
5	1.8197e−03	NA	5.5240e−03	NA	2.3704e−01	NA
10	4.7976e−04	1.9233	1.4501e−03	1.9296	1.1271e−01	1.0726
20	1.1915e−04	2.0095	3.7080e−04	1.9674	5.1155e−02	1.1396
40	2.9911e−05	1.9941	9.4230e−05	1.9764	2.4874e−02	1.0402
80	7.4878e−06	1.9980	2.3649e−05	1.9944	1.2160e−02	1.0325
160	1.8734e−06	1.9989	5.9242e−06	1.9971	6.0057e−03	1.0177

Table 2
Broken H^1 interpolation errors in the velocity for Example 4.1.

N	$\|\epsilon(u_1)\|_{1,\Omega}$	Order	$\|\epsilon(u_2)\|_{1,\Omega}$	Order
5	3.0294e−02	NA	4.6821e−02	NA
10	1.5541e−02	0.9629	2.3890e−02	0.9707
20	7.7082e−03	1.0117	1.1949e−02	0.9995
40	3.8663e−03	0.9954	5.9991e−03	0.9940
80	1.9319e−03	1.0010	3.0026e−03	0.9985
160	9.6557e−04	1.0006	1.5021e−03	0.9992

and the pressure is defined as follows:

$$p = \begin{cases} \dfrac{15(-43+4\sqrt{30})(\nu^-)^2 - 2\nu^+(310+3\sqrt{30}+30(-43+4\sqrt{30})\sqrt{0.3}+2400x))}{1200\nu^-} \\ \quad + \dfrac{\nu^-(620+6\sqrt{30}+60(-43+4\sqrt{30})\sqrt{0.3}-15\nu^+(-43+4\sqrt{30}+320x))}{1200\nu^-}, \quad \text{if } (x,y)\in T^+, \\ \dfrac{15(37+4\sqrt{30})(\nu^-)^2 - 2\nu^+(310+3\sqrt{30}+30(37+4\sqrt{30})\sqrt{0.3}+2400x+2400y)}{(1200)\nu^-} \\ \quad + \dfrac{\nu^-(620+6\sqrt{30}+60(37+4\sqrt{30})\sqrt{0.3}-15\nu^+(37+4\sqrt{30}+320x)+4800y)}{(1200)\nu^-}, \quad \text{if } (x,y)\in T^-, \end{cases} \tag{4.2b}$$

with $\nu^- = 1$, $\nu^+ = 10$ and $\boldsymbol{\sigma} = 0$. We compute interpolation errors on uniform Cartesian meshes having $N^2 = 5^2, 10^2, 20^2, 40^2, 80^2, 160^2$ square elements and present L^2 interpolation errors in Table 1. Broken H^1 interpolation errors for the velocity are shown in Table 2.

This numerical example suggests that the proposed Q_1/Q_0 IFE spaces maintain optimal convergence rates of standard Q_1/Q_0 spaces for Stokes problems with continuous viscosity and Stokes interface problems on fitted meshes in [37].

Example 4.2. We consider the domain $\Omega = [-1, 1]^2$ cut by the circular interface $x^2 + y^2 = 0.3$ that separates Ω into two regions $\Omega^+ = \{(x, y)^t : x^2 + y^2 > 0.3\}$ and $\Omega^- = \{(x, y)^t : x^2 + y^2 < 0.3\}$. The functions $\mathbf{u}$ and p are chosen to satisfy jump conditions (1.1f) and (1.1g) and are given by

$$\mathbf{u} = \begin{cases} u_1 = \begin{cases} \dfrac{y(x^2+y^2-0.3)}{\nu^+}, & \text{if } (x,y)\in T^+, \\ \dfrac{y(x^2+y^2-0.3)}{\nu^-}, & \text{if } (x,y)\in T^-, \end{cases} \\ u_2 = \begin{cases} \dfrac{x(x^2+y^2-0.3)}{\nu^+}, & \text{if } (x,y)\in T^+, \\ \dfrac{x(x^2+y^2-0.3)}{\nu^-}, & \text{if } (x,y)\in T^-, \end{cases} \end{cases} \tag{4.3a}$$

Table 3
L^2 interpolation errors for Example 4.2.

N	$\|\epsilon(u_1)\|_{0,\Omega}$	Order	$\|\epsilon(u_2)\|_{0,\Omega}$	Order	$\|\epsilon(p)\|_{0,\Omega}$	Order
5	1.4558e−02	NA	1.4108e−02	NA	4.1366e−02	NA
10	5.0590e−03	1.5249	5.1297e−03	1.4595	4.4358e−02	−0.1
20	1.7205e−03	1.5560	1.7307e−03	1.5676	1.4987e−02	1.5655
40	4.5919e−04	1.9057	4.5938e−04	1.9136	6.4336e−03	1.2200
80	1.2019e−04	1.9338	1.2021e−04	1.9341	2.9964e−03	1.1024
160	3.1002e−05	1.9549	3.1004e−05	1.9550	1.4293e−03	1.0680

Table 4
Broken H^1 interpolation errors for Example 4.2.

N	$\|\epsilon(u_1)\|_{1,\Omega}$	Order	$\|\epsilon(u_2)\|_{1,\Omega}$	Order
5	1.5794e−01	NA	1.6076e−01	NA
10	9.2499e−02	7.7182e−01	1.2743e−01	3.3517e−01
20	5.4598e−02	7.6058e−01	7.3561e−02	7.9273e−01
40	2.8592e−02	9.3322e−01	3.9815e−02	8.8563e−01
80	1.4954e−02	9.3512e−01	2.1346e−02	8.9931e−01
160	7.5775e−03	9.8071e−01	1.1152e−02	9.3671e−01

and the pressure is defined as follows:

$$p = \frac{1}{10}(x^3 - y^3) \tag{4.3b}$$

where $\nu^- = 1$, $\nu^+ = 10$ and $\boldsymbol{\sigma} = 0$.

Next we compute interpolation errors on uniform Cartesian meshes having $N^2 = 5^2, 10^2, 20^2, 40^2, 80^2, 160^2$ square elements and present L^2 interpolation errors in Table 3. Broken H^1 interpolation errors for the velocity are shown in Table 4. Here we also observe optimal quadratic convergence for the velocity and linear convergence for the pressure. We recall that the circular interface is approximated by a piecewise linear interface.

Example 4.3. We consider the same domain and interface as in the previous example and define the functions $\mathbf{u}$ and p that satisfy the homogeneous jump condition (1.1g) and a nonhomogeneous (1.1f):

$$\mathbf{u} = \begin{cases} u_1 = \begin{cases} u_1^+ = 1 - \dfrac{y}{\nu^+}\sin(0.3 - x^2 - y^2) \\ u_1^- = 1 - \dfrac{y}{\nu^-}\sin(0.3 - x^2 - y^2) \end{cases} \\ u_2 = \begin{cases} u_2^+ = 2 + \dfrac{x}{\nu^+}\sin(0.3 - x^2 - y^2) \\ u_2^- = 2 + \dfrac{x}{\nu^-}\sin(0.3 - x^2 - y^2) \end{cases} \end{cases} \tag{4.4a}$$

$$p = \begin{cases} p^+ = e^{x+y} - 1.3798535909816816 \\ p^- = \sqrt{1 + x^2 + y^2} - 1.3798535909816816. \end{cases} \tag{4.4b}$$

We select $\nu^- = 1$ and $\nu^+ = 10$ and compute the IFE interpolation errors on uniform rectangular meshes and show the interpolation errors and their orders of convergence in Tables 5 and 6. Again, the numerical results suggest that our IFE spaces maintain the optimal convergence rates in the presence of singularity across the interface.

4.2. *Convergence of the immersed finite element method*

We use numerical results to show the approximation capability of our finite element method. First we recall from [37] that using the finite element spaces Q_1/Q_0 on fitted meshes the L^2 errors of the velocity and pressure,

Table 5
L^2 interpolation errors for Example 4.3.

N	$\|\epsilon(u_1)\|_{0,\Omega}$	Order	$\|\epsilon(u_2)\|_{0,\Omega}$	Order	$\|\epsilon(p)\|_{0,\Omega}$	Order
5	9.3316e−03	NA	8.5520e−03	NA	5.4423e−01	NA
10	4.2952e−03	1.1194	4.2914e−03	0.9948	2.7921e−01	0.9628
20	1.5979e−03	1.4266	1.5976e−03	1.4255	1.4036e−01	0.9922
40	4.3181e−04	1.8877	4.3180e−04	1.8875	7.0920e−02	0.9848
80	1.1374e−04	1.9246	1.1374e−04	1.9247	3.5400e−02	1.0025
160	2.9448e−05	1.9495	2.9448e−05	1.9495	1.7721e−02	0.9982

Table 6
Broken H^1 interpolation errors for Example 4.3.

N	$\|\epsilon(u_1)\|_{1,\Omega}$	Order	$\|\epsilon(u_2)\|_{1,\Omega}$	Order
5	7.1608e−02	NA	6.7556e−02	NA
10	5.7846e−02	0.3079	5.7818e−02	0.2245
20	4.3107e−02	0.4242	4.3103e−02	0.4237
40	2.3170e−02	0.8956	2.3170e−02	0.8955
80	1.1938e−02	0.9566	1.1938e−02	0.9566
160	6.1789e−03	0.9502	6.1789e−03	0.9501

Table 7
L^2 IFE errors for SIPG method applied to Example 4.4.

N	$\|e(u_1)\|_{0,\Omega}$	Order	$\|e(u_2)\|_{0,\Omega}$	Order	$\|e(p)\|_{0,\Omega}$	Order
5	3.3087e−03	NA	3.8791e−03	NA	2.5120e−01	NA
10	9.0140e−04	1.8760	8.7783e−04	2.1437	1.0615e−01	1.2427
20	2.2736e−04	1.9872	2.0301e−04	2.1124	4.9161e−02	1.1105
40	5.7379e−05	1.9864	4.8446e−05	2.0671	2.3896e−02	1.0407
80	1.4565e−05	1.9780	1.1897e−05	2.0258	1.1894e−02	1.0065
160	3.6736e−06	1.9873	2.9492e−06	2.0122	5.9394e−03	1.0019

Table 8
Broken H^1 IFE errors for SIPG applied to Example 4.4.

N	$\|e(u_1)\|_{1,\Omega}$	Order	$\|e(u_2)\|_{1,\Omega}$	Order
5	3.2948e−02	NA	4.9512e−02	NA
10	1.6537e−02	0.9945	2.4719e−02	1.0021
20	7.9295e−03	1.0604	1.2108e−02	1.0297
40	3.9223e−03	1.0155	6.0275e−03	1.0063
80	1.9478e−03	1.0099	3.0099e−03	1.0019
160	9.7012e−04	1.0056	1.5042e−03	1.0007

respectively, are $O(h^2)$ and $O(h)$ convergent. Furthermore, the broken H^1 error of the velocity is $O(h)$ convergent. The finite element errors are denoted by $e(u_i) = u_i - u_{i,h}$ for $i = 1, 2$ and $e(p) = p - p_h$.

Example 4.4. First we consider the Stokes problem where the exact solution is given by (4.2) with a linear interface on $[-1, 1]^2$ with $\nu^- = 1$ and $\nu^+ = 10$. We use the meshes from Example 4.1 to carry out several simulations by solving (3.12a) with SIPG and NIPG methods using immersed Q_1/Q_0 spaces. We present the L^2 IFE errors in Tables 7 and 9 and the broken H^1 errors in Tables 8 and 10. The computational results show optimal quadratic convergence for the velocity and linear convergence for the pressure. The broken H^1 errors show linear convergence for the velocity.

Example 4.5. Here we consider the Stokes interface problem on $[-1, 1]^2$ with a circular interface and exact solution given by (4.3) with $\nu^- = 1$ and $\nu^+ = 10$. We solve (3.12a) using SIPG and NIPG methods on the uniform meshes

Table 9
L^2 IFE errors for NIPG method applied to Example 4.4.

N	$\|e(u_1)\|_{0,\Omega}$	Order	$\|e(u_2)\|_{0,\Omega}$	Order	$\|e(p)\|_{0,\Omega}$	Order
5	3.4272e−03	NA	3.9838e−03	NA	2.7117e−01	NA
10	9.0967e−04	1.9136	8.8799e−04	2.1655	1.1021e−01	1.2990
20	2.2703e−04	2.0025	2.0535e−04	2.1125	4.9935e−02	1.1421
40	5.5829e−05	2.0238	4.8465e−05	2.0830	2.4162e−02	1.0473
80	1.4108e−05	1.9845	1.1846e−05	2.0325	1.1953e−02	1.0154
160	3.5698e−06	1.9825	2.9313e−06	2.0148	5.9517e−03	1.0059

Table 10
Broken H^1 IFE errors for NIPG method applied to Example 4.4.

N	$\|e(u_1)\|_{1,\Omega}$	Order	$\|e(u_2)\|_{1,\Omega}$	Order
5	3.3416e−02	NA	4.9495e−02	NA
10	1.6596e−02	1.0097	2.4617e−02	1.0076
20	7.9550e−03	1.0609	1.2093e−02	1.0255
40	3.9165e−03	1.0223	6.0254e−03	1.0050
80	1.9458e−03	1.0092	3.0094e−03	1.0016
160	9.6965e−04	1.0049	1.5040e−03	1.0006

Table 11
L^2 IFE errors for SIPG method applied to Example 4.5.

N	$\|e(u_1)\|_{0,\Omega}$	Order	$\|e(u_2)\|_{0,\Omega}$	Order	$\|e(p)\|_{0,\Omega}$	Order
5	2.0045e−02	NA	2.0122e−02	NA	5.6755e−01	NA
10	6.6060e−03	1.6014	6.6230e−03	1.6032	2.8468e−01	0.9954
20	1.6771e−03	1.9778	1.6788e−03	1.9800	1.4354e−01	0.9878
40	4.2978e−04	1.9643	4.2983e−04	1.9656	7.1163e−02	1.0123
80	1.1222e−04	1.9373	1.1217e−04	1.9381	3.5401e−02	1.0073
160	2.7808e−05	2.0127	2.7795e−05	2.0128	1.7677e−02	1.0020

Table 12
Broken H^1 IFE errors for SIPG method applied to Example 4.5.

N	$\|e(u_1)\|_{1,\Omega}$	Order	$\|e(u_2)\|_{1,\Omega}$	Order
5	1.4788e−01	NA	1.4740e−01	NA
10	8.6853e−02	0.7678	8.6677e−02	0.7660
20	4.7526e−02	0.8698	4.7488e−02	0.8681
40	2.4497e−02	0.9561	2.4490e−02	0.9553
80	1.2395e−02	0.9828	1.2394e−02	0.9825
160	6.2400e−03	0.9901	6.2396e−03	0.9901

from the previous example with the IFE Q_1/Q_0 spaces. We present the L^2 errors in Tables 11 and 13 while the H^1 errors are shown in Tables 12 and 14. The numerical results again suggest quadratic convergence for the velocity and linear convergence for the pressure in the L^2 norm. The errors in broken H^1 show linear convergence for the velocity.

The computational results show that, despite the presence of the singularity, the L^2 errors in the velocity and pressure for the interior penalty IFE methods maintain the optimal orders of convergence shown in [37] for both $\mathbf{u}$ and p.

Example 4.6. We solve the Stokes interface problem on $[-1, 1]^2$ with the true solution (4.4) with nonzero surface force using SIPG and NIPG methods with our IFE spaces on uniform rectangular meshes and show the IFE errors and convergence orders in Tables 15–18. Again, the numerical results show that our immersed Q_1/Q_0 interior penalty

Table 13
L^2 IFE errors of NIPG method applied to Example 4.5.

N	$\|e(u_1)\|_{0,\Omega}$	Order	$\|e(u_2)\|_{0,\Omega}$	Order	$\|e(p)\|_{0,\Omega}$	Order
5	1.5657e−02	NA	1.5274e−02	NA	3.6065e−01	NA
10	4.6777e−03	1.7430	4.7450e−03	1.6866	2.3837e−01	0.5974
20	1.2919e−03	1.8563	1.2980e−03	1.8702	9.6466e−02	1.3051
40	3.4281e−04	1.9140	3.4302e−04	1.9199	3.5601e−02	1.4381
80	9.1878e−05	1.8996	9.1895e−05	1.9002	1.2834e−02	1.4719
160	2.2674e−05	2.0187	2.2676e−05	2.0188	4.6366e−03	1.4689

Table 14
Broken H^1 IFE errors of NIPG method applied to Example 4.5.

N	$\|e(u_1)\|_{1,\Omega}$	Order	$\|e(u_2)\|_{1,\Omega}$	Order
5	1.5691e−01	NA	1.5949e−01	NA
10	9.0996e−02	0.7860	1.2474e−01	0.3546
20	5.4141e−02	0.7490	7.2397e−02	0.7849
40	2.8510e−02	0.9252	3.9634e−02	0.8691
80	1.4935e−02	0.9328	2.1296e−02	0.8961
160	7.5725e−03	0.9798	1.1135e−02	0.9354

Table 15
L^2 IFE errors of SIPG method applied to Example 4.6.

N	$\|e(u_1)\|_{0,\Omega}$	Order	$\|e(u_1)\|_{0,\Omega}$	Order	$\|e(p)\|_{0,\Omega}$	Order
5	9.2041e−03	NA	8.5578e−03	NA	5.4909e−01	NA
10	4.5395e−03	1.0197	4.5505e−03	0.9112	2.7844e−01	0.9796
20	1.4915e−03	1.6057	1.4932e−03	1.6076	1.4054e−01	0.9863
40	3.9612e−04	1.9128	3.9624e−04	1.9140	7.0953e−02	0.9860
80	1.0697e−04	1.8887	1.0693e−04	1.8897	3.5401e−02	1.0031
160	2.7612e−05	1.9774	2.7613e−05	1.9775	1.4127e−03	1.0600

Table 16
Broken H^1 IFE errors of SIPG method applied to Example 4.6.

N	$\|e(u_1)\|_{1,\Omega}$	Order	$\|e(u_2)\|_{1,\Omega}$	Order
5	7.4130e−02	NA	7.1057e−02	NA
10	5.7993e−02	0.3541	5.7955e−02	0.2940
20	4.2999e−02	0.4315	4.2987e−02	0.4310
40	2.3153e−02	0.8930	2.3152e−02	0.8927
80	1.1935e−02	0.9560	1.1935e−02	0.9559
160	7.5730e−03	0.9799	1.1138e−02	0.9355

methods maintain the optimal convergence rates for the Stokes interface problem with a nonhomogeneous jump condition.

5. Conclusion

In this manuscript we presented an immersed discontinuous finite element method for solving two-dimensional Stokes interface problems that does not require the mesh to be aligned with the interface. We first showed how to design piecewise polynomial IFE shape functions and discussed their basic properties, then we constructed a discontinuous Galerkin IFE method for the Stokes interface problem. The optimal convergence rates of the proposed immersed piecewise polynomial spaces and finite element methods have been tested computationally by computing

Table 17
L^2 IFE errors of NIPG method applied to Example 4.6.

N	$\|e(u_1)\|_{0,\Omega}$	Order	$\|e(u_2)\|_{0,\Omega}$	Order	$\|e(p)\|_{0,\Omega}$	Order
5	9.2914e−03	NA	8.6753e−03	NA	5.4880e−01	NA
10	3.5277e−03	1.3972	3.5297e−03	1.2973	2.8385e−01	0.9511
20	1.0441e−03	1.7564	1.0436e−03	1.7580	1.4428e−01	0.9762
40	2.8611e−04	1.8676	2.8597e−04	1.8677	7.2363e−02	0.9955
80	7.8308e−05	1.8693	7.8220e−05	1.8702	3.5822e−02	1.0144
160	1.9256e−05	2.0238	1.9228e−05	2.0243	1.7832e−02	1.0064

Table 18
Broken H^1 IFE errors of NIPG method applied to Example 4.6.

N	$\|e(u_1)\|_{1,\Omega}$	Order	$\|e(u_2)\|_{1,\Omega}$	Order
5	7.3792e−02	NA	7.0814e−02	NA
10	5.7363e−02	0.3633	5.7322e−02	0.3049
20	4.2973e−02	0.4166	4.2966e−02	0.4158
40	2.3151e−02	0.8923	2.3151e−02	0.8921
80	1.1935e−02	0.9559	1.1934e−02	0.9559
160	6.1779e−03	0.9499	6.1779e−03	0.9499

interpolation errors and by solving Stokes interface problems with linear and circular interfaces. In the future we intend to carry out an error analysis to establish theoretical bounds for both the interpolation and the finite element errors for the Stokes interface problem.

Acknowledgment

This research was partially supported by the National Science Foundation (Grant Number DMS 1016313).

References

[1] I. Babuska, J.E. Osborn, Can a finite element method perform arbitrarily badly?, Math. Comp. 69 (2000) 443–462.
[2] J.H. Bramble, J.T. King, A finite element method for interface problems in domains with smooth boundary and interfaces, Adv. Comput. Math. 6 (1997) 109–138.
[3] Z. Chen, J. Zou, Finite element methods and their convergence for elliptic and parabolic interface problems, Numer. Math. 79 (1998) 175–202.
[4] A. Quarteroni, A. Valli, Domain Decomposition Methods for Partial Differential Equations, Oxford, New York, 1999.
[5] J. Brackbill, D. Kothe, C. Zemach, A continuum method for modeling surface tension, J. Comput. Phys. 100 (1992) 335–354.
[6] R. Ausas, F. Sousa, G. Buscaglia, An improved finite element space for discontinuous pressures, Comput. Methods Appl. Mech. Engrg. 199 (2010) 1019–1031.
[7] A. Reusken, Analysis of an extended pressure finite element space for two-phase incompressible flows, Comput. Visual Sci. 11 (2008) 293–305.
[8] T.P. Fries, T. Belytschko, The extended/generalized finite element method: An overview of the method and its applications, Internat. J. Numer. Methods Engrg. 84 (2010) 253–304.
[9] R. Becker, E. Burman, P. Hansbo, A Nitsche extended finite element method for incompressible elasticity with discontinuous modulus of elasticity, Comput. Methods Appl. Mech. Engrg. 198 (2009) 3352–3360.
[10] P. Hansbo, M. Larson, S. Zahedi, A cut finite element method for a Stokes interface problem, Appl. Numer. Math. 85 (2014) 90–114.
[11] V. Girault, B. Riviere, M. Wheeler, A discontinuous Galerkin method with non-overlapping domain decomposition for the Stokes and Navier Stokes problems, Math. Comp. 74 (2005) 53–84.
[12] A. Layton, J. Beale, On the accuracy of finite difference methods for elliptic problems with interfaces, Commun. Appl. Math. Comput. Sci. 1 (2006) 91–119.
[13] R.J LeVeque, Z. Li, The immersed interface method for elliptic equations with discontinuous coefficients and singular sources, SIAM J. Numer. Anal. 31 (1994) 1019–1044.
[14] R.J LeVeque, Z. Li, Immersed interface methods for Stokes flow with elastic boundaries or surface tension, SIAM J. Sci. Comput. 18 (1997) 709–735.
[15] Z. Li, The immersed interface method a numerical approach for partial differential equations with interfaces (Ph.D. thesis), University of Washington, 1994.
[16] Z. Li, K. Ito, The Immersed Interface Method, SIAM, Philadelphia, 2006.
[17] Z. Li, W. Wang, I. Chern, M. Lai, New formulations for interface problems in polar coordinates, SIAM J. Sci. Comput. 25 (2003) 224–245.

[18] Z. Li, K. Ito, M. Lai, An augmented approach for Stokes equations with a discontinuous viscosity and singular forces, Comput. & Fluids 36 (2007) 622–635.
[19] S. Adjerid, T. Lin, Higher-order immersed discontinuous Galerkin methods, Int. J. Inf. Syst. Sci. 3 (2007) 558–565.
[20] S. Adjerid, T. Lin, A p^{th}-degree immersed finite element method for boundary value problems with discontinuous coefficients, Appl. Numer. Math. 59 (2009) 1303–1321.
[21] S. Adjerid, M. Ben Romdhane, T. Lin, High-order interior penalty immersed finite element method for second-order elliptic interface problems, Int. J. Numer. Anal. Model. 11 (2014) 541–566.
[22] B. Camp, T. Lin, Y. Lin, W.-W. Sun, Quadratic immersed finite element spaces and their approximation capabilities, Adv. Comput. Math. 24 (2006) 81–112.
[23] Y. Gong, B. Li, Z. Li, Immersed-interface finite element methods for elliptic interface problems with non-homogeneous jump conditions, SIAM J. Numer. Anal. 46 (2008) 472–495.
[24] X. He, T. Lin, Y. Lin, Approximation capability of a bilinear immersed finite element space, Numer. Methods Partial Differential Equations 24 (2008) 1265–1300.
[25] R. Kafafy, T. Lin, Y. Lin, J. Wang, 3-D immersed finite element methods for electric field simulation in composite materials, Internat. J. Numer. Methods Engrg. 64 (2005) 904–972.
[26] Z. Li, The immersed interface method using a finite element formulation, Appl. Numer. Math. 27 (1998) 253–267.
[27] Z. Li, T. Lin, Y. Lin, R. Rogers, An immersed finite element space and its approximation capability, Numer. Methods Partial Differential Equations 20 (2004) 338–367.
[28] Z. Li, T. Lin, X. Wu, New Cartesian grid methods for interface problems using finite element formulation, Numer. Math. 96 (2003) 61–98.
[29] T. Lin, Y. Lin, R.C. Rogers, L.M. Ryan, A rectangular immersed finite element method for interface problems, in: P. Minev, Y. Lin (Eds.), in: Advances in Computation: Theory and Practice, vol. 7, Nova Science Publishers, Inc., 2001, pp. 107–114.
[30] S. Adjerid, N. Chaabane, T. Lin, P. Yue, A Q_1/Q_0 immersed finite element method for the Stokes problem with a moving interface, 2015, in preparation.
[31] T. Lin, X. Zhang, Linear and bilinear immersed finite elements for planar elasticity interface problems, J. Comput. Appl. Math. 236 (2012) 4681–4699.
[32] X. He, T. Lin, Y. Lin, Immersed finite element methods for elliptic interface problems with non-homogeneous jump conditions, Int. J. Numer. Anal. Model. 8 (2011) 284–301.
[33] B. Cockburn, G. Kanschat, D. Schötzau, C. Schwab, Local discontinuous Galerkin methods for the Stokes system, SIAM J. Numer. Anal. 40 (2002) 319–343.
[34] D. Schötzau, C. Schwab, A. Toselli, Mixed *hp*-DGFEM for incompressible flows, SIAM J. Numer. Anal. 40 (2002) 2171–2194.
[35] P. Hansbo, M.G. Larson, Discontinuous Galerkin methods for incompressible and nearly incompressible elasticity by Nitsche method, Comput. Methods Appl. Mech. Engrg. 191 (2002) 1895–1908.
[36] A. Toselli, *hp* discontinuous Galerkin approximations for the Stokes problem, Math. Models Methods Appl. Sci. 12 (2002) 1565–1597.
[37] B. Riviere, Discontinuous Galerkin Methods for Solving Elliptic and Parabolic Equations, Frontiers in Applied Mathematics, Philadelphia, 2008.
[38] R.L. Burden, J.D. Faires, Numerical Analysis, tenth ed., Brooks, Cole, 2015.